Volume 61
Number 25
28 March 2025
Pages 4729–4870

ChemComm

Chemical Communications

rsc.li/chemcomm

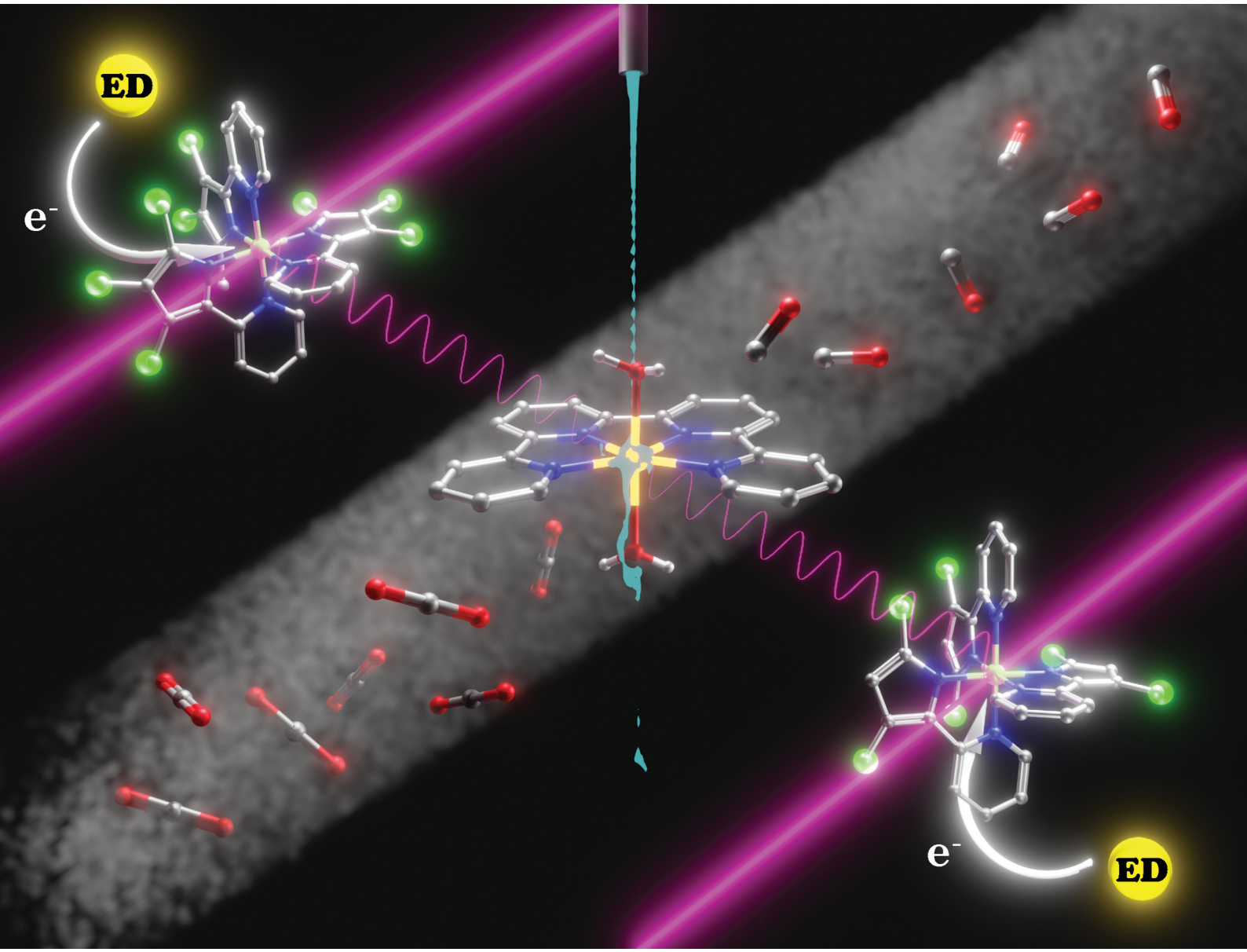

ISSN 1359-7345

ROYAL SOCIETY OF CHEMISTRY

COMMUNICATION

Jia-Wei Wang, Dooshaye Moonshiram *et al.*
Femto-microsecond electron transfer and intermediates in Al/Fe CO_2 photoreduction systems through optical and X-ray spectroscopy

ChemComm

COMMUNICATION

View Article Online
View Journal | View Issue

Cite this: *Chem. Commun.*, 2025, **61**, 4788

Received 3rd December 2024,
Accepted 13th February 2025

DOI: 10.1039/d4cc06404f

rsc.li/chemcomm

Femto-microsecond electron transfer and intermediates in Al/Fe CO_2 photoreduction systems through optical and X-ray spectroscopy†

Maxime Sauvan,[a] Ashok Ugale,[a] Lucia Velasco,[ab] Asterios Charisiadis,[a] Fan Ma,[c] Xiaoyi Zhang,[d] Jia-Wei Wang *[c] and Dooshaye Moonshiram *[a]

This study reveals the reaction pathways of 2 Al–Fe earth-abundant photocatalytic systems for CO_2 reduction through femto-nanosecond optical transient absorption and microsecond X-ray spectroscopies. Time-resolved experimental findings with time-dependent density functional theory illustrate the formation of an elusive Fe^{I} octahedral species with bound aqua ligands and lifetimes of 23–29 μs.

The increasing burning of fossil fuels has over the past decades resulted in an increasing CO_2 concentration that is responsible for today's global warming. The photochemical transformation of CO_2 into natural gases or liquid fuels, using water as an abundant electron donor, could not only generate renewable fuels[1] but also mitigate greenhouse gas emissions. The reduction of CO_2 is, however, not a trivial process and requires proton-assisted multiple electron transfer steps[2] that can further outcompete H_2 formation. Multielectron–proton reactions can effectively be achieved through redox-photosensitizer, catalytic systems[3] that can couple transient one-electron excited states in the presence of an electron donor to the catalyst. An efficient and selective CO_2 reduction catalyst with multiple electrons can subsequently react with CO_2 and release reduction products while avoiding side proton reduction reactions. Rare noble photosensitizers composed of Re,[4] Os[5] or Ru[6] centres have extensively been employed in homogeneous CO_2-reduction photocatalysis. The lack of efficient noble-metal-free photosensitizers has further prompted the development of exclusively earth-abundant metal complexes, such as binuclear Cu(I) complexes[7] composed of two tetradentate ligands which achieved photocatalytic CO_2 reduction in the presence of either Fe or Mn catalysts.[8] Such families of Cu photosensitizers have, however, been known to display the formation of a flattened geometry within their excited states that enables nucleophilic attack by solvent molecules or counter anions. As a result, low-energy excited states known as an "exciplex"[9,10] that decay to the ground state within microsecond time scales are formed, limiting their stabilities during photocatalysis.

In the search for a larger library of economical CO_2 photocatalytic systems, multimolecular assemblies composed of a $[Fe^{II}(qpy)(OH_2)_2]^{2+}$ (qpy = 2,2′:6′,2″:6″,2‴-quaterpyridine) catalyst and Al-based photosensitizers featuring monoanionic 2-pyridyloyrrolide ligands[11,12] with varying number of methyl ligands denoted here as **Al-1** and **Al-2** (Scheme 1) were further explored in the presence of a BIH (1,3-dimethyl-2-phenyl-2,3,dihydro-1*H*-benzo[*d*]imidazole) electron donor and TEOA (triethanolamine) (Scheme 1). Al-based complexes represent for instance an interesting class of earth-abundant photosensitizers with an earth abundance of 14 000 ppm[13] and have been less explored for photophysical and photochemical applications. The noble-metal-free Al/Fe systems were further shown to display ligand–ligand charge transfer (LLCT) excited states,[11] impressive turnover numbers of 10 250 for CO formation and higher robustness than benchmarking Cu and Ru photosensitizers, thus providing a promising platform for CO_2 reduction. A complete photocatalytic system composed of Ru or Cu based photosensitizers

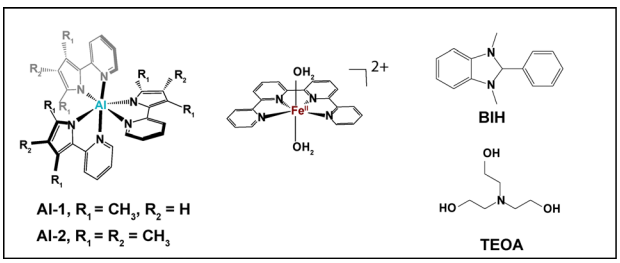

Scheme 1 Structure of the Al photosensitizers and Fe catalyst studied in a multimolecular system with a BIH electron donor and a TEOA proton donor and acceptor.

[a] *Instituto de Ciencia de Materiales de Madrid (ICMM-CSIC), Sor Juana Inés de la Cruz, 3, Madrid, 28049, Spain. E-mail: dooshaye.moonshiram@csic.es*
[b] *Departamento de Química Física, Universidad Complutense de Madrid, Avenida Complutense s/n, Madrid, E-28040, Spain*
[c] *School of Chemical Engineering and Technology, Sun Yat-sen University, Zhuhai, 519082, China. E-mail: wangjw89@mail.sysu.edu.cn*
[d] *X-ray Science Division, Argonne National Laboratory, 9700 S. Cass Avenue, Lemont IL, 60439, USA*

† Electronic supplementary information (ESI) available: Experimental section, EXAFS analysis, time-resolved XAS kinetics, and DFT optimization. See DOI: https://doi.org/10.1039/d4cc06404f

with the Fe catalyst under the same experimental conditions for instance showed much lower turnover numbers of 401 and 72, respectively.[11] Importantly, the excited states were found to be a singlet in nature while the triplet excited states displayed non-emissive behaviors.

Although the photophysics of the Al photosensitizers (Scheme 1) together with their catalytic activities were probed, the kinetics along with the electronic and structural conformation of the Fe catalyst upon photoexcitation with the Al photosensitizers were elusive, yet of crucial importance for the development of cost-effective photocatalytic systems for durable CO_2 reduction. In this regard, femto-nanosecond optical transient absorption (OTA) and pico-microsecond time-resolved X-ray absorption spectroscopy (tr-XAS, Fig. S1, ESI†) are employed herein to investigate the formation of the Al excited states and electron transfer events to generate the active Fe^{I} species. The structural conformation of the Fe^{I} reduced state responsible for CO_2 reduction is further corroborated with time-dependent density functional theory calculations (TD-DFT). This work provides valuable insights into the overall mechanistic scenario of a family of earth-abundant molecular photocatalytic systems crucial for the development of artificial photosynthetic assemblies for CO_2 utilization.

Prior to investigating a full photocatalytic system through time-resolved spectroscopy, steady state X-ray absorption near edge structure (XANES) and extended X-ray absorption fine structure (EXAFS) measurements were carried out to compare the coordination behaviours and structural conformations of the Fe catalyst in solid *vs.* solution (Fig. 1). The XAS measurements were conducted at 15 K with a defocused beam to minimize radiation damage (Fig. 1). The XANES spectra of the Fe catalyst in the solid and solution states display K-edge energies of 7123.1 eV and 7123.6 eV, respectively at half height and normalized fluorescence of 0.6 consistent with an Fe^{II} oxidation state[14] (Fig. 1A). Although the Fe complex maintains the same oxidation state in both the solid and solution states, a small shift in the XANES rising edge of 0.5 eV (Fig. 1A) together with a decrease in the pre-edge intensities (Fig. 1A inset) is observed upon dissolution in a mixture of 0.93 : 0.07 CH_3CN : DMF suggesting a change in the local Fe symmetries. A small amount of DMF was employed to match the same solvent experimental conditions as OTA and tr-XAS experiments elaborated below.

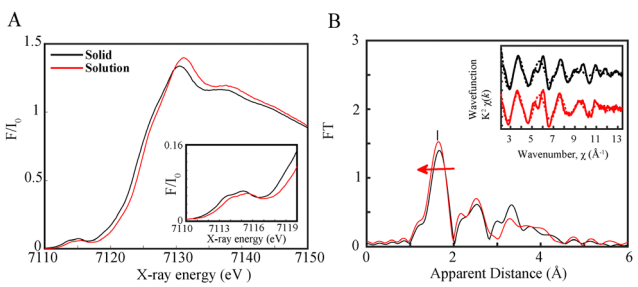

Fig. 1 (A) Normalized Fe K-edge XANES spectra of 1 mM of the FeQPY catalyst in solid (black) and a solution mixture of 0.93 : 0.07 CH_3CN : DMF. Inset: Zoomed-in view of the pre-edge features. (B) Experimental Fourier transforms of k^2-weighted Fe EXAFS of the FeQPY solid and solution complex (1 mM). Inset: Back Fourier transforms experimental (solid lines) and fitted (dashed lines) Re[$\chi(k)$]. Experimental spectra were calculated for k values of 2.118 to 13.443 $Å^{-1}$.

The Fe^{II} catalyst in a $3d^6$ high spin distorted octahedral geometry has 4 unpaired electrons, 2 in each one of its t_{2g} and e_g levels thus leading to broad multiplet pre-edge features with peak energies at 7112.6 and 7114.2 eV (Fig. 1A inset). The presence of pre-edge features corresponds to the weak 1s to 3d quadrupole transitions which gain intensity through the dipole excitations of the core electrons into the valence 3d states hybridized with the N/C ligand p orbitals.[15] Interestingly, the Fe catalyst in solution displays a small decrease in its pre-edge intensity confirming a more centrosymmetric coordination environment than that in the solid state (Fig. 1A inset). Indeed, complexes in a centrosymmetric coordination have been shown to exhibit weaker pre-edge features than non-centrosymmetric complexes.[14] The trends in the pre-edge features further rule out the formation of a distorted Fe^{II} complex bound to only one water or solvent molecule.

To further assess the structural conformation of the Fe catalyst upon dissolution, DFT optimization calculations were carried out using the BP86 functional in the gas phase and through the conductor-like polarizable models for the solid and solution complexes, respectively, as elaborated in the ESI.† Several possible geometries were theoretically explored and the best agreement between both the pre-edge and rising edge features was found for an Fe^{II} complex bound strongly to two aqua ligands in solution (Fig. S2, ESI†).

The EXAFS spectrum of the catalyst in the solid and solution states further displays a prominent peak I corresponding to the average contribution of the Fe–N/O bond distances (Fig. 1B). The EXAFS fits for the extraction of the actual distances are shown in Fig. 1B inset, Fig. S2 and Table S1 (ESI†). Analysis of the first peak for the Fe solid complex clearly resolves 6 Fe–N distances at 2.15 Å (Table S1 and Fig. S3, ESI†), in perfect agreement with its X-ray diffraction (XRD) analysis and DFT calculations conducted in the gas phase (Table S2, Appendix, ESI†). By contrast, the Fe complex in CH_3CN:DMF reveals six slightly shortened Fe–N bond distances at 2.13 Å in agreement with the DFT structure of the optimized complex in solution phase (Table S1 and Fig. S3, ESI†). The shortened Fe–N distances and six-coordinated geometry explain its shifted XANES spectra *vs.* its solid spectrum, and thus slightly larger energy is needed to eject a core 1s electron. The extracted bond distances for the catalyst in solution additionally rules out the formation of a Fe^{II} complex ligated with a single CH_3CN, single aqua or a square planar Fe^{II} geometry whereby averaged Fe–N bond distances of 2.09, 2.10 and 2.08 Å (Table S2, Appendix, ESI†) would be respectively expected. Importantly theoretical methods including geometrical optimizations and XANES simulations reproduce the experimental EXAFS analysis well showing that they can be employed to deduce the structural conformation of the photoinduced catalytic species.

Following steady state XAS spectra of the catalyst, optical transient absorption was carried out to probe the electron transfer events in both Al photosensitizers separately (Fig. 2) as well as in a complete photocatalytic system with the Fe catalyst, BIH and TEOA (Fig. 3). The TEOA can in this case function both as a proton acceptor for the deprotonation reaction of BIH and as a proton donor for the facilitation of the CO_2 reduction reaction as previously shown.[11] The **Al-1** and **Al-2** photosensitizers with (2-(3,5-dimethyl-1*H*-pyrrol-2-yl)pyridine) and (2-(3,4,5,trimethyl,1*H*,pyrrol,2-yl)pyridine) ligands

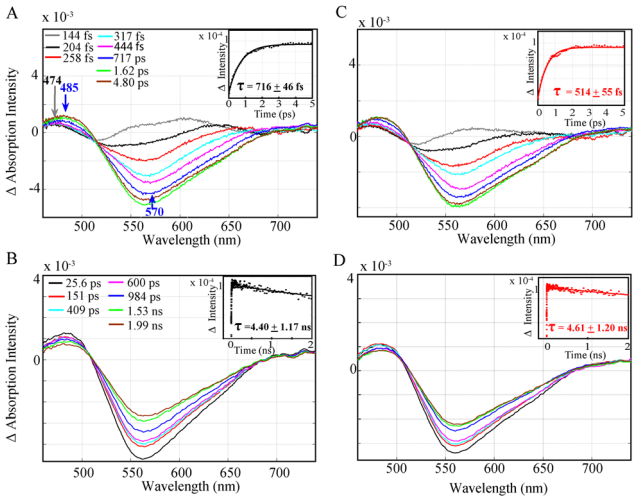

Fig. 2 OTA spectra of a solution of (A) 0.3 mM **Al-1**, (C). 0.3 mM **Al-2** in 0.93 : 0.07 CH_3CN : DMF upon light excitation at 355 nm between pump-probe delays from 144 fs up to 4.80 ps. Insets (A) and (C): kinetic decay profiles at λ = 485 nm after excitation at λ_{exc} = 355 nm illustrating the formation of the singlet excited state. OTA spectra of a solution of (B) 0.3 mM **Al-1**, (D) 0.3 mM **Al-2** in 0.93 : 0.07 CH_3CN : DMF upon light excitation at 355 nm between 25.6 ps and 1.99 ns. Insets (B) and (D): kinetic decay profiles at λ = 485 nm after excitation at λ_{exc} = 355 nm illustrating the intersystem crossing rate from the singlet to the triplet.

containing 2 and 3 methyl groups respectively were designed to serve as π-acceptors for the stabilization of the metal reduced states in a photocatalytic system.

Both **Al-1** and **Al-2** were known to exhibit a broad absorption band above 350 nm peaking around 393 and 405 nm, respectively.[11] Upon laser excitation at 355 nm, a broad negative absorption between 520 nm and 700 nm with a maximum peak at 570 nm is observed due to stimulated emission (Fig. 2A and C). A broad positive peak at around 485 nm can further be seen corresponding to the formation of the singlet excited state. The singlet excited state **Al*** was found to occur faster and within 514 ± 55 fs in **Al-2** (Fig. 2C and Fig. S3, ESI†) *vs.* 716 ± 46 fs in **Al-1** (Fig. 2A and Fig. S4, ESI†) due to the presence of more electron donating methyl groups which play an important role in populating the excited state. By contrast, the intersystem crossing rate from the singlet to the triplet excited state occurs at a slower nanosecond rate within 4.40 ± 1.17 ns (Fig. 2B) and 4.61 ± 1.20 ns (Fig. 2D) in **Al-1** and **Al-2,** respectively, in agreement with previous findings.[11] Our femto-sub nanosecond laser measurement did not allow observation of the microsecond-lived triplet absorption found[11] in the range of 430 to 500 nm.

Nevertheless, the study of a complete photocatalytic system with the Fe catalyst, excess BIH and TEOA shows that an emissive singlet excited state is effectively quenched for **Al-1** and **Al-2** within 1.24 ± 0.140 ns (Fig. 3A) and 1.19 + 0.260 ns (Fig. 3B) respectively, thus illustrating the reductive quenching of the photosensitizers singlet excited states to be the dominant pathway for photoinduced catalysis. Previous work[11] has shown that the lifetimes of the **Al** photosensitizers could only be dynamically quenched by BIH rather than the Fe catalyst. However, while the OTA measurements effectively illustrate the quenching of the singlet excited states, the formation of the reduced $\mathbf{Al}^-$ state or photocatalytic Fe^I species could not be observed due to their overlapping absorption bands with the stimulated emission together with the lower extinction coefficient of the photocatalyst.

Time-resolved XANES was thus applied to monitor the kinetics and electronic configurations of the photo-induced Fe^I in a complete photocatalytic system. The multimolecular Al/Fe photocatalytic systems were optically pumped at 400 nm and probed with X-ray pulses from 100 ps to ~25 μs (Fig. 4 and Fig. S5A, ESI†). Upon light excitation, low lying LLCT initially occurs to form a singlet excited state followed by the BIH electron donor quenching to generate a reduced $\mathbf{Al}^-$ state. This process is followed by an electron transfer from the $\mathbf{Al}^-$ reduced state to the Fe^{II} catalyst, generating the elusive Fe^I species (Fig. 4A).

The time-resolved XANES spectra obtained by subtracting the laser-ON and laser-OFF (dark) spectra provided valuable information about the photo-induced dynamics, electronic and structural nature of the photoinduced Fe^I. The time resolved XANES spectrum at an averaged delay of 14.2 μs between the laser pump excitation and X-ray probing for both photocatalytic mixtures composed of **Al-1** and **Al-2** is shown in Fig. 4A. The transient signals display a time-dependent broad peak at 7123.5 eV together with a dip at 7148 eV which is related to the characteristic formation of the reduced Fe^I species and ground state bleaching of the Fe^{II} ground state, respectively (Fig. 4A). These two transitions further show that the Fe^{II} K-edge energy shifts to lower energy upon photoexcitation thus confirming the effective electron transfer process from the reduced $\mathbf{Al}^-$ state to the Fe^I catalyst. It is also important to note that no transient signals were observed in the absence of the BIH electron donor thus showing that the electron donor is indeed essential to quench the singlet excited state **Al*** to generate $\mathbf{Al}^-$ which thereby transfers an electron to the Fe catalyst.

It should be mentioned that the excited state fractions of the photoreduced Fe^I was too low (less than 5%), to reconstruct the EXAFS and structural conformation. Tr-XANES spectra were thus next combined with TD-DFT to extract the structural conformation of the photo-generated Fe^I species (Fig. 4B). Several Fe^I geometries were considered namely an Fe^I complex coordinated with 2 aqua (black), another with 2 CH_3CN (red) or with 1 aqua and 1 CH_3CN (cyan) ligand (Fig. 4B). A square bipyramidal Fe^I complex with a single aqua (magenta) or CH_3CN (blue) ligand, as well as a square planar Fe^I geometry (green), were also considered. The best agreement between the experimental trends and best energy matching was obtained for an Fe^I species with 2 elongated aqua molecules at

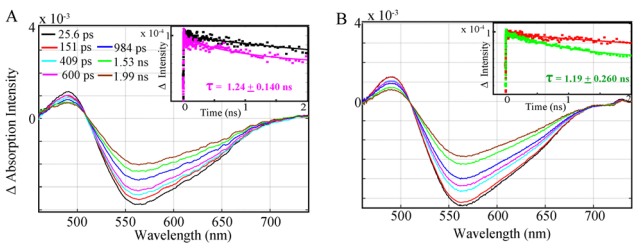

Fig. 3 OTA spectra of a complete photocatalytic system of (A) 0.3 mM **Al-1** and (B) 0.3 mM **Al-2** with 0.3 mM Fe catalyst, 30 mM BIH and 30 mM TEOA in 0.93 : 0.07 CH_3CN : DMF. Insets (A) and (B): quenching of the $\mathbf{Al}^-$ singlet excited state by BIH to generate the reduced optically silent $\mathbf{Al}^-$ reduced species.

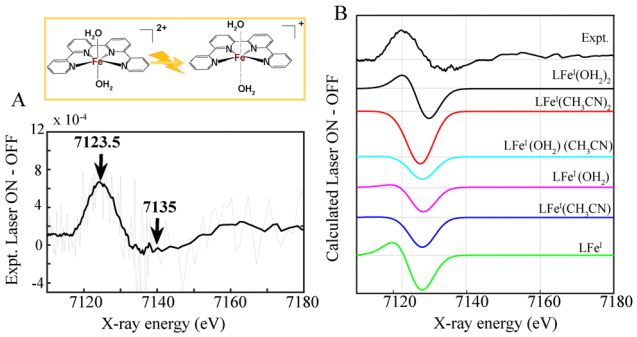

Fig. 4 Top: formation of a photoreduced Fe^{I} species with 2 loosely coordinated molecules for a multimolecular assembly composed of the 2.5 mM **Al-1** or **Al-2** photosensitizer, 1 mM FeQPY catalyst, 100 mM BIH and 100 mM TEOA in a solution mixture of 0.93 : 0.07 CH_3CN : DMF. A small amount of DMF is added to improve the solubility of the Al-based photosensitizers used in 2.5 mM concentrations. (A) Experimental laser ON–OFF spectra corresponding to formation of Fe^{I} at 14.2 μs (B). Experimental laser ON–OFF spectrum (black) in comparison with theoretical XANES simulations corresponding to the formation of a [LFe^{I}–$(OH_2)_2$] (black), [LFe^{I}–$(CH_3CN)_2$], [LFe^{I}–(OH_2) (CH_3CN)] (cyan) octahedral complex, a square bipyramidal [LFe^{I}–OH_2] (magenta), [LFe^{I}–CH_3CN] (blue) and a [LFe^{I}] square planar photoreduced species (blue) from [LFe^{II}–$(OH_2)_2$].

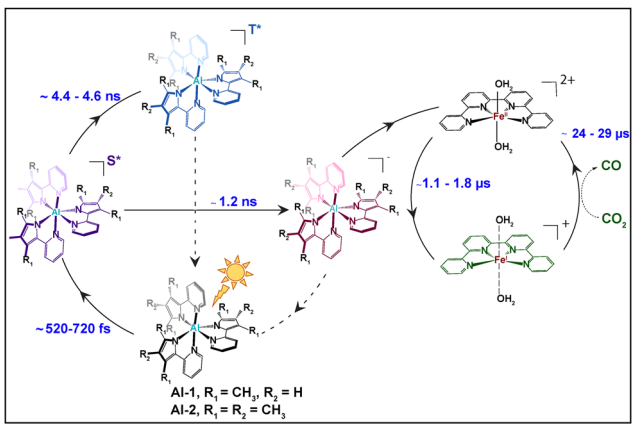

Scheme 2 Mechanistic pathways for the photoexcitation reaction of Al photosensitizers **Al-1** and **Al-2** followed by electron transfer reaction to the Fe-based CO_2 reduction catalyst.

2.29 Å (Fig. 4 and Table S2, Appendix, ESI†) which would allow coordination and activation of a CO_2 molecule. The progressions and decays of the transient signals for both photocatalytic systems composed of **Al-1** and **Al-2** photosensitizers were further analysed at successive time points ranging from 2.75 to 25.7 μs (Fig. S5, ESI†). The Fe^{I} reduced species was shown to be formed within 1.02–1.72 μs and decay within 23.2–28.9 μs in both photocatalytic systems (Fig. S5, ESI†). In summary, we report the application of femto-picosecond optical as well as pico-microsecond X-ray spectroscopy together with TD-DFT calculations to monitor the electronic and structural dynamics of the elusive Fe^{I} species in two sets of earth-abundant robust and selective Al–Fe multimolecular systems for CO_2 reduction (Scheme 2). Upon light excitation in a complete photocatalytic system, LLCT initially triggers the formation of a singlet excited state within 716 fs and 514 fs, respectively, in **Al-1** and **Al-2** followed by an electron transfer to BIH within 1.2 ns to form the reduced $\mathbf{Al}^{-}$ state (Scheme 2 and Fig. 2A, B and 3). The **Al*** excited state is notably formed faster in **Al-2** due to the presence of more electron donating methyl groups. The reduced $\mathbf{Al}^{-}$ species subsequently transfers an electron to the Fe^{II} catalyst within 1.1–1.7 μs to form a long-lived Fe^{I} species with lifetimes of 23 to 29 μs (Scheme 2 and Fig. 4 and Fig. S5, ESI†). The singlet excited states were further shown to display intersystem crossing rates of 4.4–4.6 ns in the absence of BIH and TEOA (Fig. 2C and D and Scheme 2) showing that the reductive quenching of the singlet is the predominant pathway. These findings report for the first time the mechanistic scenario and structure of the elusive Fe^{I} species in a fuly noble metal-free molecular system for CO_2 reduction and thus constitute an important step for the future design of robust and durable earth-abundant photosensitizer/catalytic assemblies.

D. M. acknowledges funding from Spanish Ministerio de Ciencia, Innovación y Universidades grants (TED2021-1327 57B-I00, PID2022-143013OB-I00).

Data availability

The data supporting this article have been included in the ESI.†

Conflicts of interest

There are no conflicts to declare.

Notes and references

1 E. E. Benson, C. P. Kubiak, A. J. Sathrum and J. M. Smieja, *Chem. Soc. Rev.*, 2009, **38**, 89–99.
2 F. Droghetti, A. Amati, F. Pascale, A. Crochet, M. Pastore, A. Ruggi and M. Natali, *ChemSusChem*, 2024, **17**, e202300737.
3 H. Kumagai, Y. Tamaki and O. Ishitani, *Acc. Chem. Res.*, 2022, **55**, 978–990.
4 T. Morimoto, C. Nishiura, M. Tanaka, J. Rohacova, Y. Nakagawa, Y. Funada, K. Koike, Y. Yamamoto, S. Shishido, T. Kojima, T. Saeki, T. Ozeki and O. Ishitani, *J. Am. Chem. Soc.*, 2013, **135**, 13266–13269.
5 Y. Tamaki, K. Koike, T. Morimoto, Y. Yamazaki and O. Ishitani, *Inorg. Chem.*, 2013, **52**, 11902–11909.
6 H. Ishida, K. Fujiki, T. Ohba, K. Ohkubo, K. Tanaka, T. Terada and T. Tanaka, *J. Chem. Soc. Dalton Trans.*, 1990, 2155–2160.
7 H. Takeda, Y. Monma and O. Ishitani, *ACS Catal.*, 2021, **11**, 11973–11984.
8 H. Takeda, H. Kamiyama, K. Okamoto, M. Irimajiri, T. Mizutani, K. Koike, A. Sekine and O. Ishitani, *J. Am. Chem. Soc.*, 2018, **140**, 17241–17254.
9 S.-P. Luo, E. Mejía, A. Friedrich, A. Pazidis, H. Junge, A.-E. Surkus, R. Jackstell, S. Denurra, S. Gladiali, S. Lochbrunner and M. Beller, *Angew. Chem., Int. Ed.*, 2013, **52**, 419–423.
10 L. Velasco, L. Llanos, P. Levín, A. Vega, J. Yu, X. Zhang, L. Lemus, D. Aravena and D. Moonshiram, *Phys. Chem. Chem. Phys.*, 2021, **23**, 3656–3667.
11 J. W. Wang, F. Ma, T. Jin, P. He, Z. M. Luo, S. Kupfer, M. Karnahl, F. Zhao, Z. Xu, T. Jin, T. Lian, Y. L. Huang, L. Jiang, L. Z. Fu, G. Ouyang and X. Y. Yi, *J. Am. Chem. Soc.*, 2023, **145**, 676–688.
12 V. Caliskanyürek, A. Riabchunova, S. Kupfer, F. Ma, J.-W. Wang and M. Karnahl, *Inorg. Chem.*, 2024, **63**, 15829–15840.
13 J. W. Morgan and E. Anders, *Proc. Natl. Acad. Sci.*, 1980, **77**, 6973–6977.
14 T. E. Westre, P. Kennepohl, J. G. DeWitt, B. Hedman, K. O. Hodgson and E. I. Solomon, *J. Am. Chem. Soc.*, 1997, **119**, 6297–6314.
15 R. Sarangi, *Coord. Chem. Rev.*, 2013, **257**, 459–472.